Research Square

Preprints are preliminary reports that have not undergone peer review.
They should not be considered conclusive, used to inform clinical practice,
or referenced by the media as validated information.

Mapping long-term spatiotemporal dynamics of seagrass structure using remote sensing: A case study from Biscayne Bay, Florida

Marianna Coppola
mcopp016@fiu.edu
Florida International University
Jonathan R. Rodemann
Florida International University
W. Ryan James
Florida International University
Gina A. Badlowski
Florida International University
Sofia M. Garcia
Florida International University
Daniel Gann
Florida International University
Jennifer S. Rehage
Florida International University
Rolando O. Santos
Florida International University

Research Article

Keywords: Seagrass structure, Seagrass dynamics, Spatial pattern metrics, Time-series mapping, Satellite remote sensing

Posted Date: November 16th, 2026

DOI: https://doi.org/10.21203/rs.3.rs-11578597/v1

License: This work is licensed under a Creative Commons Attribution 4.0 International License.
Read Full License

Additional Declarations: No competing interests reported.

Mapping long-term spatiotemporal dynamics of seagrass structure using remote sensing: A case study from Biscayne Bay, Florida

Marianna Coppola[1]*, Jonathan R. Rodemann[1], W. Ryan James[1,2,3], Gina A. Badlowski[1], Sofia M. Garcia[1], Daniel Gann[1], Jennifer S. Rehage[2,3], Rolando O. Santos[1,3]

[1] Department of Biological Sciences, Florida International University, Miami, USA
[2] Department of Earth and Environment, Florida International University, Miami, USA
[3] Institute of Environment, Florida International University, Miami, USA

Corresponding author:
*Marianna Coppola
Email: mcopp016@fiu.edu
Phone: +1 561-817-9544

ORCID:
Marianna Coppola: mcopp016@fiu.edu ORCID: 0009-0005-7264-4627
Jonathan R. Rodemann: rodemann@nceas.ucsb.edu ORCID: 0009-0006-9740-8599
W. Ryan James: wjames@fiu.edu ORCID: 0000-0002-4829-7742
Gina A. Badlowski: gina.badlowski1@fiu.edu ORCID: 0000-0001-6830-1131
Sofia M. Garcia: sgarc510@fiu.edu ORCID: 0009-0006-7802-7774
Daniel Gann: gannd@fiu.edu ORCID: 0000-0001-6131-3391
Jennifer S. Rehage: rehagej@fiu.edu ORCID: 0000-0003-0009-6906
Rolando O. Santos: rsantosc@fiu.edu ORCID: 0000-0002-3885-9406

Abstract

Context Seagrass seascapes respond to environmental variability and disturbance through changes in habitat composition and spatial configuration. Long-term satellite archives provide opportunities to track these dynamics using remote sensing techniques.

Objectives We tested whether a consistent classification model can be successfully applied through a Sentinel-2 time series to reconstruct submerged aquatic vegetation (SAV) dynamics in Biscayne Bay, Florida, from 2016 to 2025. We assessed how SAV composition, seagrass cover, configuration varied across space and time.

Methods Annual maps were generated across a ten-year satellite data time series. SAV dynamics were characterized through pixel-level transitions, bay-wide composition, and spatial patterns of dense seagrass amount and fragmentation, including net and cumulative changes.

Results Systematic annual mapping revealed spatially heterogeneous SAV dynamics across Biscayne Bay, despite the absence of significant bay-wide trends in habitat composition for any benthic class. At the pixel level, compositional transitions were concentrated primarily along the western margin of the bay, where historical disturbances have influenced habitat dynamics. Changes in dense seagrass cover and fragmentation exhibited an inverse relationship, with increasing cover generally associated with declining fragmentation and vice versa. Importantly, areas exhibiting net changes only partially overlapped with those experiencing cumulative changes, particularly in fragmentation, highlighting the complex dynamics of seascape configuration and spatial rearrangement over time.

Conclusions A consistent classification framework can be systematically applied across satellite archives to reconstruct seagrass trajectories in coastal systems. Integrating time series habitat maps with spatial pattern metrics can reveal localized dynamics and intermediate structural changes, providing a repeatable approach for long-term seascape monitoring.

Keywords Seagrass structure; Seagrass dynamics; Spatial pattern metrics; Time-series mapping; Satellite remote sensing.

Introduction

Seagrass meadows are crucial components of coastal ecosystems worldwide, supporting biodiversity and fisheries while contributing to carbon sequestration, sediment stabilization, water clarity, and coastal protection (Boström et al., 2011; Herrera-Silveira et al., 2024; Waycott et al., 2009). Seagrass can respond to natural or human-induced disturbances rapidly over periods of a few weeks to months, making them particularly valuable as biological indicators in monitoring and conservation programs (O'Brien et al., 2018; Roca et al., 2016). Seagrass habitats are inherently spatially heterogeneous and organized into discrete patches or larger meadows. Together with other benthic habitat types, seagrasses form complex seascape mosaics whose structure is defined by the spatial distribution, arrangement, and relationships among habitat elements (Wedding et al., 2011; Yarnall et al., 2022). Habitat composition and configuration provide complementary dimensions for characterizing seascape structure. Composition describes the abundance and diversity of habitat types within a seascape, whereas configuration captures their spatial arrangement by measuring structural characteristics such as patch shape complexity, isolation, and edge structure (McGarigal, 1995a). Importantly, composition and configuration operate independently, so that seascapes with similar seagrass cover may differ in spatial organization and, consequently, ecological function (Fahrig et al., 2011; Frazier & Kedron, 2017; Santos et al., 2016).

Seagrass habitats display compositional and configurational dynamics driven by the interplay of environmental disturbance regimes (Uhrin & Turner, 2018). Examining the structural dimensions of seagrass meadows through time can reveal processes of habitat loss, fragmentation, expansion, and coalescence, as well as spatially heterogeneous trajectories of decline, persistence, and recovery (Fernandes et al., 2022; Rodemann et al., 2021). For example, a significant decline in seagrass cover over time indicates habitat loss, while decreasing patch size and increasing patch number and isolation reflect fragmentation (Jensen & Bell, 2001; Sleeman et al., 2005; Yarnall et al., 2022). When habitat loss and fragmentation occur simultaneously, they may signal progressive habitat degradation, characterized by both a reduction in habitat extent and decreasing connectivity, which can in turn trigger destabilizing positive feedback loops, exacerbating undesired ecosystem conditions (Heide et al., 2010; Taylor et al., 2026). However, these trajectories may vary locally within the same coastal system, with some areas exhibiting habitat recovery while others undergo continued loss, fragmentation, and degradation (Rodemann et al., 2025).

Because seagrasses are sensitive to changes in environmental conditions, including water quality, light availability, and nutrient enrichment, changes in their distribution, abundance, and spatial configuration can serve as indicators of coastal ecosystem health (Roca et al., 2016). Thus, effective resource management depends on monitoring approaches that adequately track the spatiotemporal patterns and dynamics of habitat structure. Satellite remote sensing has been increasingly applied to generate habitat maps that are suitable to quantify structural heterogeneity across coastal environments (Hossain et al., 2015; Rowan & Kalacska, 2020; Traganos et al., 2022). The growing availability of multispectral satellite data, along with advances in remote sensing techniques, has made seagrass habitat mapping increasingly widespread over the last two decades, supporting applications across diverse coastal regions and spatiotemporal scales (Krause et al., 2021; Roelfsema et al., 2014; Traganos et al., 2018). These developments have expanded mapping approaches from delineating seagrass presence and extent to distinguishing variation in habitat cover, type, and benthic composition using a range of sensors and analytical techniques (Knudby & Nordlund, 2011; Pu et al., 2010).

Drawing on landscape ecology, habitat maps consist of spatially explicit digital products that provide the basis for deriving spatial pattern metrics (SPMs), algorithms that quantify habitat compositional and configurational characteristics (Kupfer, 2012; McGarigal, 1995b). In coastal systems, integrating categorical benthic habitat maps with SPMs allows us to quantify seascape structural properties across hierarchical levels of organization, i.e., at the patch, class, and landscape level (Pittman, 2017; Wedding et al., 2011). When calculated from a single habitat map, SPMs measure habitat structure at a given point in time; however, deriving consistent metrics from multiple maps representing the same system at different time points has proven effective in providing insight into the seascape of structural change (Cunha & Santos, 2009; Rodemann et al., 2025; Sleeman et al., 2005). Although comparisons between individual time points capture net changes in habitat structure, longer intervals between observations may obscure intervening dynamics, including habitat loss followed by recovery or repeated spatial reorganization.

Open Earth-observation satellite archives enable repeated seagrass habitat mapping across large coastal systems, providing the temporal coverage needed to reconstruct habitat trajectories at spatial and temporal scales difficult to achieve through field surveys alone (Coffer et al., 2023; Veettil et al., 2020). In terrestrial ecosystems, continuous

satellite time series have been successfully used to reconstruct landscape trajectories, revealing long-term dynamics that are not captured by comparisons among isolated time points (Kennedy et al., 2010). Whether similarly automated time-series approaches can effectively characterize habitat trajectories remains less established in coastal systems, where mapping submerged habitats is complicated by water-column effects, variable optical conditions, and spectral similarities among benthic cover classes (Rowan & Kalacska, 2020).

Long-term monitoring of seagrass habitats is essential to understand their responses to environmental pressures and disturbances and to inform coastal management, conservation, and restoration efforts. However, the limited availability of long-term, high-resolution seagrass habitat maps remains a major data gap, limiting our ability to characterize spatially variable responses to changing environmental conditions and identify areas of both seagrass recovery and decline. Given the substantial analytical effort required to process and classify extensive satellite image archives, we tested whether continuous mapping provides valuable insights into seascape spatiotemporal dynamics beyond what can be obtained from fewer individual time points. To address these gaps, we integrated Sentinel-2 imagery with field observations to generate annual benthic habitat maps of Biscayne Bay, Florida (USA), from 2016 to 2025. We developed a consistent classification framework to distinguish seagrass density and co-occurring macroalgal habitats, generating thematically consistent annual maps to quantify seagrass structural patterns and dynamics by independently addressing both composition and configuration.

Specifically, we addressed three research questions: (1) How did seagrass habitat composition and configuration change over the study period? (2) How did these changes vary spatially across Biscayne Bay? And (3) does annual mapping reveal temporal variability and habitat reorganization beyond endpoint comparison? We hypothesized that changes in seagrass cover and fragmentation would be more pronounced along the western bay margin, where freshwater inputs contribute to pronounced habitat changes. We further expected that seagrass dynamics would not follow exclusively linear trajectories, but would include periods of decline, recovery, and repeated spatial reorganization, resulting in cumulative changes that could exceed the net differences observed between endpoints.

Methods

Study site

Biscayne Bay is a shallow subtropical lagoon in southern Florida (USA; Figure 1), where extensive seagrass habitats co-occur with macroalgal assemblages, collectively referred to as submerged aquatic vegetation (SAV), across pronounced spatial gradients in environmental conditions (Lirman et al., 2014). The northwestern portion of the bay borders the highly urbanized Miami metropolitan area, while its western shoreline receives freshwater inputs through an extensive network of drainage canals. To the east, barrier islands and limestone keys separate the bay from the Atlantic Ocean, with tidal inlets connecting it to adjacent marine waters. Over the past century, urban development and profound hydrological modifications have altered the bay's natural freshwater and nutrient delivery, replacing diffuse freshwater inputs with localized canal discharges that have disrupted historical salinity and nutrient gradients (Browder & Ogden, 1999; Lirman & Cropper, 2003). Additionally, climate change and sea-level rise have introduced further environmental pressures, including rising water temperatures and declining pH across most monitored zones (Caccia et al., 2026). These cumulative stressors, together with macroalgal blooms, have impacted seagrass habitats, which experenced extensive die-offs in northern Biscayne Bay (Alexandre et al., 2021; Carbonell et al., 2021; Santos et al., 2020).

SAV surveys

Visual inspection of the multispectral image stacks described in the previous section indicated substantial spectral similarity among SAV types and cover levels, limiting their reliable discrimination from imagery alone. *In situ* observations were therefore used to characterize spectral properties of benthic habitats and define classes based on measured vegetation cover and composition, reducing uncertainty associated with spectral overlap among habitats. Ground-truthing surveys were conducted across Biscayne Bay to provide field observations for both classification model training and independent accuracy assessment of the final SAV maps.

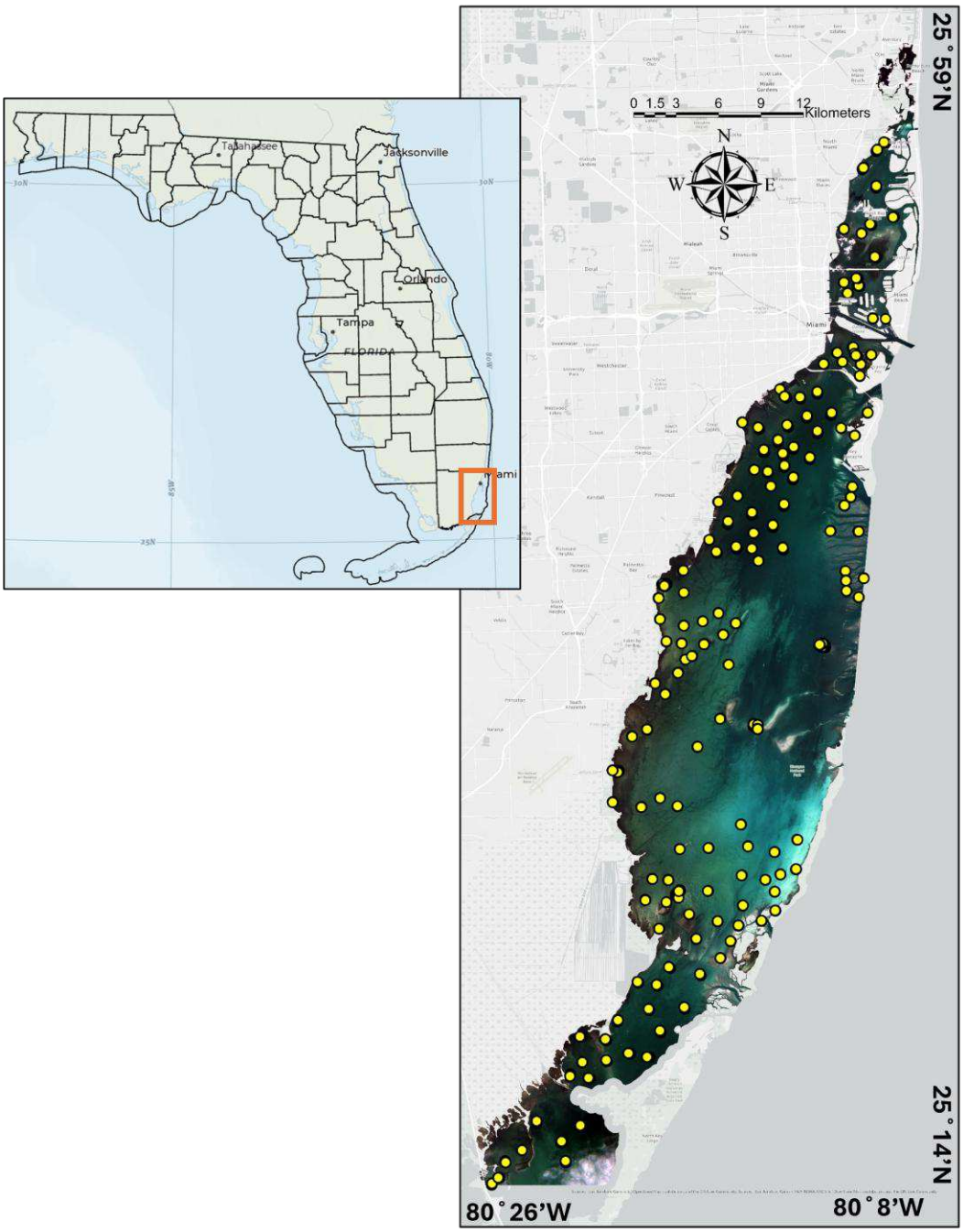


Figure 1: Biscayne Bay study area. Yellow points represent SAV survey sites.

At each sampling location, a 1 m² PVC quadrat was deployed on the benthos and photographed to document SAV composition and cover, resulting in 368 photoquadrats in 2023, 687 in 2024, and 634 in 2025. The geographic position of each quadrat was recorded at its center using a Satellite-Based Augmentation System (SBAS)-corrected Global Navigation Satellite System (GNSS), with an average positional accuracy of 20–70 cm. Two sampling designs were employed during the study period. In 2023 and 2024, a systematic transect-based design was used, in which two 30 m transects were deployed in a cross-configuration intersecting at their midpoints (15 m), with quadrats placed at the intersection and at each transect end. In 2025, the sampling design was modified to improve field efficiency by deploying a quadrat at the initial site and subsequently relocating it ten times along the prevailing

water current direction, with placements spaced approximately 10–20 m apart. Photoquadrats were visually scored for percent cover of individual seagrass species, major macroalgal genera, and sessile invertebrates. Cover estimates were then aggregated to derive total benthic percent cover (TOT), total seagrass cover (TSG), and total macroalgal cover (TMA).

Satellite data acquisition and atmospheric correction

Sentinel-2 imagery provided the primary input for the remote sensing workflow used in this study to generate annual benthic habitat maps and quantify temporal changes in seagrass structure (Figure 2).

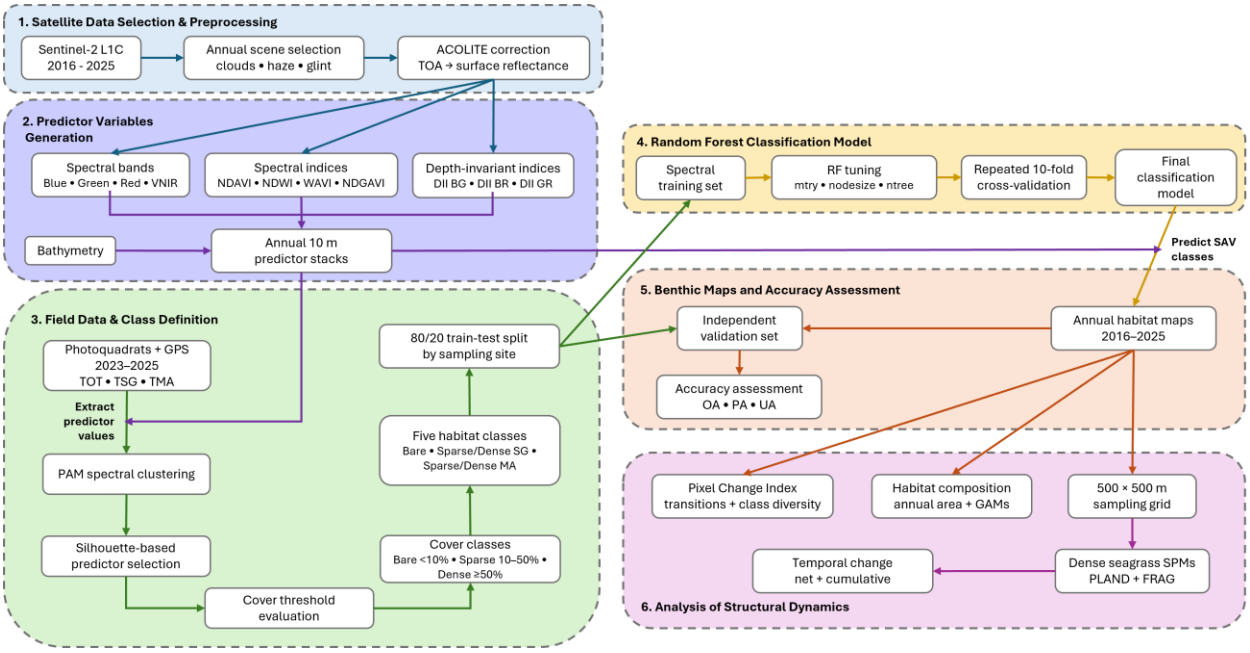


Figure 2: Schematic illustration of methods used to generate annual benthic habitat maps and quantify seagrass structural dynamics in Biscayne Bay. The workflow includes satellite preprocessing, predictor generation, field-based class definition, Random Forest classification and accuracy assessment, and temporal seascape analyses.

Sentinel-2 satellite imagery was selected due to its 10-meter spatial resolution in the visible and near-infrared bands, 5-day revisit cycle, freely available multispectral archive, and suitability for seagrass mapping based on previous studies (Floyd et al., 2026; Kuhwald et al., 2022; Traganos et al., 2018). All image querying, visualization, and export workflows were implemented in R using the rgee package (Aybar & Stigler, 2021), which provides direct access to the Google Earth Engine (GEE) API. For each year (2016–2025), Sentinel-2 Level 1-C (L1C) Top-of-Atmosphere (TOA) imagery (COPERNICUS/S2_HARMONIZED) was accessed via GEE and filtered to the T17RNJ Tile, which encompasses the majority of the Biscayne Bay area of interest (AOI). We applied no cloud-cover threshold at the image-collection level, ensuring all potential candidate scenes were retained for visual evaluation. Each annual image collection was then manually inspected on a scene-by-scene basis directly within the rgee interactive mapping interface. Image selection was based on visual assessment of (1) cloud and cirrus presence over the AOI, (2) atmospheric artifacts including haze and sun glint, and (3) overall visibility of benthic features (e.g., seagrass beds and substrate heterogeneity). Within each year, all available scenes were compared, and a single representative image was selected and exported based on optimal conditions. Finally, the selected TOA scenes (Online Supplementary Material Table. S1) were atmospherically corrected to surface reflectance using the dark spectrum fitting algorithm available in the ACOLITE processor (Vanhellemont & Ruddick, 2016), which is specifically designed for optically complex coastal waters.

Image pre-processing

To strenghten the discrimination between benthic habitat classes, we generated a suite of spatial predictor layers from atmospherically corrected Sentinel-2 imagery in R using the terra package (Hijmans, 2020). Initial spectral

characterization included computation of univariate statistics (mean, variance) for data quality inspection and inter-band multivariate relationships using Pearson correlation matrices to assess multicollinearity, inform predictor calculations, and enhance benthic habitat discrimination. Three spectral indices: NDAVI, NDWI, and WAVI were computed following formulations described by Rowan & Kalacska (2020), and a two-band ratio index was computed as NDGAVI based on the Pearson correlation matrix. To reduce the influence of water-column attenuation on benthic reflectance, three depth-invariant indices (DIIs) were calculated following the approach of Lyzenga et al. (2006). Bare substrate locations were visually identified and digitized in ArcGIS Pro, and their blue, green, red, and VNIR reflectance values were extracted and log-transformed. Band pairs exhibiting linear relationships among log-transformed reflectance values were retained for depth-invariant transformation. For each retained band pair i,j, the ratio of attenuation coefficients was estimated from the variance and covariance of the log-transformed reflectance values as:

$$a = \frac{\mathrm{Var}(X_i) - \mathrm{Var}(X_j)}{2\mathrm{Cov}(X_i, X_j)} \qquad (1)$$

$$\frac{k_i}{k_j} = a + \sqrt{a^2 + 1} \qquad (2)$$

Depth-invariant transformations were then computed as Depth Invariant Indices:

$$DII_{ij} = \ln(R_i) - \frac{k_i}{k_j}\ln(R_j) \qquad (3)$$

computing blue–green, blue–red, and green–red corrected bands. In addition to spectral predictors, a bathymetric raster layer representing water depth across Biscayne Bay was also included.

10-meter raster layers generated from Sentinel-2 bands and stacked for successive analysis.

Layer	Source	Equation	Use
Blue Band (BB)	Sentinel-2	N/A	Deeper water
Green Band (GB)	Sentinel-2	N/A	Water
Red Band (RB)	Sentinel-2	N/A	Shallow water/terrestrial
Very Near Infrared (VNIR)	Sentinel-2	N/A	Terrestrial
Normalized Difference Aquatic Vegetation Index (NDAVI)	Rowan and Kalacska, 2020	$(VNIR - BB)/(VNIR + BB)$	Underwater vegetation identification
Water Adjusted Vegetation Index (WAVI)	Rowan and Kalacska, 2020	$1.5(VNIR - BB)/(VNIR + BB)$	Underwater vegetation identification
Normalized Difference Water Index (NDWI)	Rowan and Kalacska, 2020	$(GB - VNIR)/(GB + VNIR)$	Water identification
Normalized Difference Green Aquatic Vegetation Index (NDGAVI)	Pearson correlation	$(VNIR - GB)/(VNIR + GB)$	Underwater vegetation identification
BB-GB Depth-invariant Band (DII_BG)	Lyzenga et al., 2006	$BB - (K_{BB}/K_{GB})GB$	Remove effect of depth using blue and green bands
BB-RB Depth-invariant Band (DII_BR)	Lyzenga et al., 2006	$BB - (K_{BB}/K_{RB})RB$	Remove effect of depth using blue and red bands
GB-RB Depth-invariant Band (DII_GR)	Lyzenga et al., 2006	$GB - (K_{GB}/K_{RB})RB$	Remove effect of depth using green and red bands
Depth	NOAA	N/A	Depth in meters

Finally, all raster layers were then combined into multiband stacks for each year. The final predictor stacks (**?@tbl-spectral-predictors**) consisted of raw spectral bands, derived spectral indices, depth-invariant layers, and bathymetry, all co-registered at 10 m resolution. These stacks were used as inputs for subsequent classification modeling.

Classification scheme selection

To identify ecologically meaningful benthic habitat classes that could be distinguished using remotely sensed spectral information, we first evaluated whether spectral variation among field observations corresponded to differences in SAV total percent cover. Spectral values were extracted from the processed predictor stacks at field survey locations and analyzed using Partitioning Around Medoids (PAM), a k-medoids clustering algorithm that uses observed data points as cluster centers and is relatively robust to outliers (Kaufman & Rousseeuw, 2009). An initial PAM model was fitted using all 12 predictors, with the number of clusters fixed at k = 3 to explore broad spectral groupings potentially associated with bare substrate and sparse and dense SAV cover. Field-derived benthic cover measurements were excluded from clustering to ensure that spectral groups were identified independently of observed vegetation density and composition.

To isolate the predictors contributing most strongly to spectral cluster separation and reduce noise, we performed a leave-one-variable-out analysis based on average silhouette width. The silhouette width of the initial 12-predictor PAM model served as a baseline, against which models fitted after the individual removal of each predictor were compared (Figure 3 a). For each iteration, the remaining predictors were standardized, and PAM was refitted with k = 3. Negative changes in average silhouette width indicated reduced cluster separation following variable removal, suggesting a positive contribution to spectral discrimination, whereas positive changes indicated improved separation. Based on this evaluation, eight predictors were retained: blue, green, red, NDAVI, ind24, NDWI, WAVI, and DII_green_red. These variables were subsequently used to fit the reduced PAM model with k = 3, producing three spectral clusters that were assigned as bare, sparse and dense habitat conditions based on their association with field-observed SAV cover (Figure 3 b).

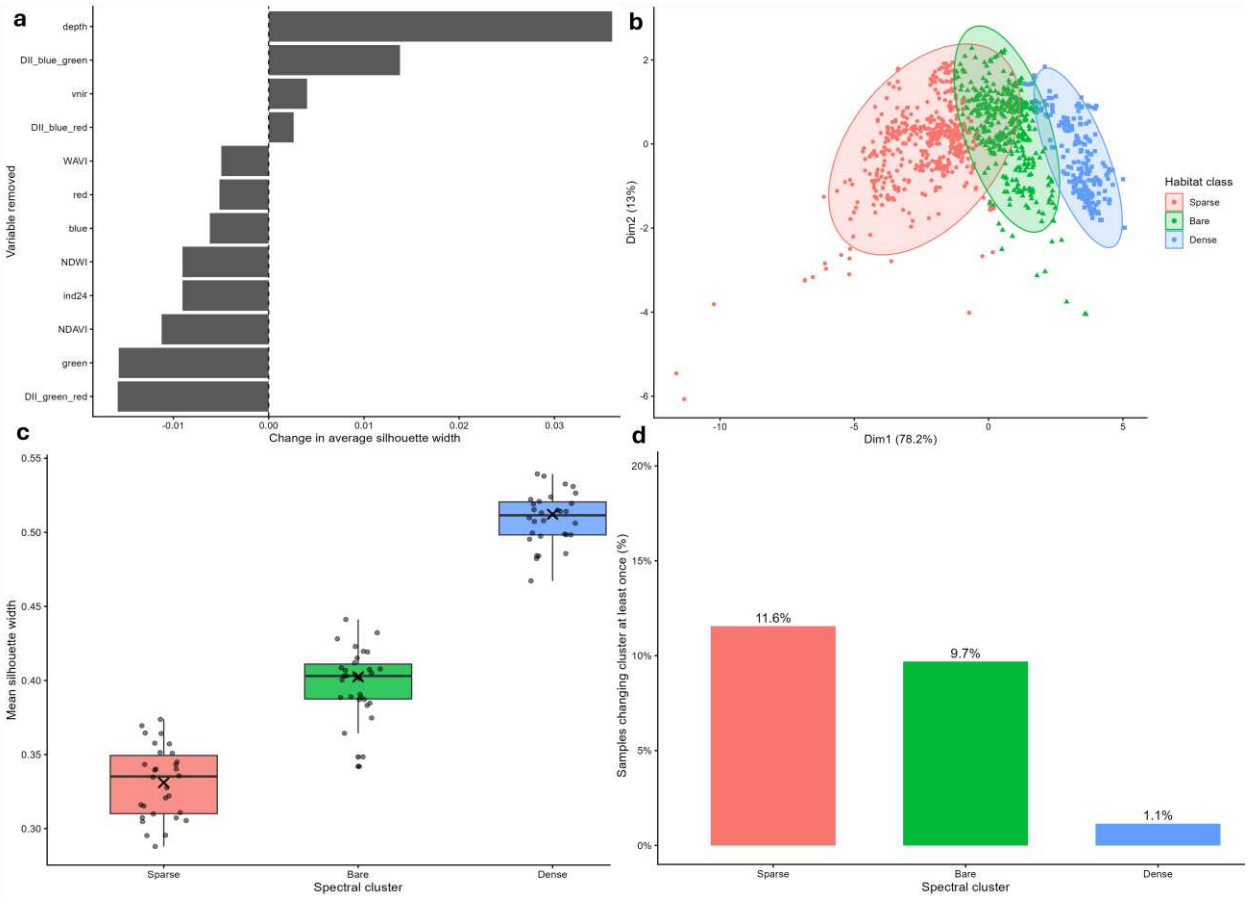


Figure 3: Spectral predictor selection and validation using Partitioning Around Medoids (PAM). (a) Change in average silhouette width following removal of individual predictors from the initial 12-variable model (k = 3), with negative values indicating reduced cluster separation. (b) Final PAM clustering using eight selected predictors, with the first two dimensions explaining 78.2% and 13.0% of variation, respectively. Clusters correspond to sparse, bare, and dense habitat conditions. (c) Cluster-specific silhouette widths across repeated three-fold cross-validation (10 repetitions); black crosses indicate full-data reference values. (d) Percentage of observations changing cluster membership at least once across 30 model fits, indicating assignment stability.

To assess the robustness of the reduced PAM clustering, we performed repeated three-fold cross-validation with ten repetitions, resulting in 30 model fits. In each cross-validation iteration, approximately two-thirds of the observations were used to fit PAM, while the remaining third was reserved for validation. Spectral predictors in both subsets were z-score standardized using the mean and standard deviation of the training data, ensuring consistent scaling while preventing information leakage from the validation subset. PAM was then fitted to the standardized training data, and validation observations were assigned to the nearest training-derived medoid using Euclidean distance. Cluster separation was assessed by calculating silhouette widths for validation observations and summarizing the mean values for each cluster across the 30 cross-validation iterations. These values were compared with those from a reference PAM model fitted to the complete dataset to evaluate the consistency of spectral separation (Figure 3 c). We additionally evaluated cluster membership stability by assigning all observations to the nearest medoids from each of the 30 fitted models and comparing their assignments across iterations. For each cluster, we calculated the percentage of observations that changed cluster membership at least once across the 30 iterations, indicating how sensitive cluster assignments were to changes in the training data (Figure 3 d).

Following PAM, the resulting cluster assignments were appended to the original field dataset to link the spectral signatures and associated clusters to SAV cover, thereby reconnecting each spectral observation with its corresponding TOT, TSG, and TMA measurements. This allowed the spectral clusters to be interpreted along a vegetation-cover gradient without incorporating field-derived cover measurements into the clustering procedure. The medoid values associated with the lowest and highest TOT were used to characterize the sparse and dense

portions of the cover gradient, respectively, while 0% cover represented bare substrate. Cover thresholds were then calculated as the midpoints between these values. Specifically, lower and upper thresholds were derived as:

$$\text{Lower threshold} = \frac{0 + \text{TOT Cluster 2 medoid}}{2} = \frac{0 + 13.3}{2} = 6.65$$

$$\text{Upper threshold} = \frac{\text{TOT Cluster 2 medoid} + \text{TOT Cluster 3 medoid}}{2} = \frac{13.3 + 100}{2} = 56.65$$

These thresholds were used to construct an initial cover-based classification scheme separating bare substrate (TOT < 6.65%), sparse SAV (6.65% ≤ TOT < 56.65%), and dense SAV (TOT ≥ 56.65%). To incorporate differences in SAV composition, we refined our classification based on the relative contribution of seagrass (TSG) and macroalgal (TMA) cover. Observations with TSG > TMA were classified as seagrass-dominated, whereas those with TMA > TSG were classified as macroalgae-dominated. Combining SAV cover and type resulted in five habitat classes: bare substrate, sparse seagrass, dense seagrass, sparse macroalgae, and dense macroalgae. The initial cover thresholds of 6.65% and 56.65% were adjusted to more interpretable values, and four alternative threshold combinations were evaluated. For each scheme, a separate Random Forest classification model was trained, and model performance was compared using out-of-bag (OOB) error estimates. Given the minimal differences in OOB error among the tested schemes, we selected thresholds of 10% and 50%, which provided ecologically meaningful distinctions among SAV cover classes, improved discrimination between low-cover SAV and bare substrate, and maintained high classification accuracy for dense seagrass. The resulting classes were defined as bare substrate (<10% cover), sparse vegetation (10–50%), and dense vegetation (>50%). The final classification assigned observations with TOT < 10% as bare substrate, those with 10% ≤ TOT < 50% as sparse vegetation, and those with TOT ≥ 50% as dense vegetation. Within the sparse and dense categories, TSG > TMA identified seagrass-dominated habitat and TMA > TSG identified macroalgae-dominated habitat. The final scheme therefore integrated total SAV cover as a measure of vegetation density and relative seagrass–macroalgae cover as a measure of habitat composition.

Random Forest Classifier and Multiclass SAV Maps

The classified spectral dataset was used as the input for a supervised machine learning classification framework. Initially, the dataset was partitioned into training and testing subsets using an 80–20% split. To reduce spatial autocorrelation and maximize the robustness of our accuracy assessment, training and testing datasets were structured such that they did not include observations from the same field survey location (sites) containing individual quadrat observations, while maintaining spatial representativeness across the area of study. A benthic habitat classification model was developed using a Random Forest classifier trained on the spectral training set predictor variables, with habitat class as the predicted variable. All analyses were conducted in R by integrating terra, sf, mlr, caret, and randomForest packages (Bischl et al., 2016; Breiman et al., 2002; Hijmans, 2020; Kuhn, 2007; Pebesma, 2018). Model tuning was conducted in two stages to optimize Random Forest performance. First, the optimal number of variables randomly selected at each split (mtry) was identified by evaluating multiple candidate models using 500 trees per iteration and selecting the configuration that minimized out-of-bag (OOB) error. Model robustness was then evaluated using repeated k-fold cross-validation (10 folds, 10 repetitions) to obtain stable performance estimates across resampled partitions. Subsequently, a secondary randomized hyperparameter tuning was performed by testing node size (nodesize) and number of trees (ntree), while holding mtry constant at its optimized value. The final Random Forest model was then back-cast through the entire time series of Sentinel-2-derived layer stacks. The resulting predictions generated annual benthic habitat maps representing the five habitat classes.

Classification accuracy was evaluated using independent field observations withheld from model training for the years in which validation data were available (2023–2025). For each year, the predicted habitat class was extracted from the classified map at the location of each validation observation and compared with its field-derived reference class. Validation observations from the three years were then pooled to provide an overall assessment of classification performance across the mapping framework. A confusion matrix was constructed for the five benthic habitat classes, from which overall accuracy (OA) and class-specific producer's (PA) and user's accuracies (UA) were calculated. Producer's accuracy quantified the proportion of reference observations within each class that were correctly classified, whereas User's accuracy quantified the proportion of observations mapped as a given class that agreed with the reference data.

Pixel Change Index

Because *in situ* observations were only available for 2023–2025, a design-based accuracy assessment could not be conducted for earlier maps. To address this limitation, we evaluated the frequency and magnitude of pixel-level class transitions across the time series as an indirect indicator of temporal classification consistency in the absence of validation data. Impossible pixel transitions, such as repeated changes in habitat classes over short intervals, may indicate classification uncertainty rather than actual habitat change. We quantify these transitions using a custom Pixel Change Index (PCI), designed to capture both the frequency of class change and the diversity of classes they were assigned to, and calculated:

$$PCI = \frac{n_{\text{trans}}}{T-1} \times \frac{n_{\text{unique}}}{K-1} \qquad (4)$$

where n_{trans} is the number of class transitions, n_{unique} is the number of unique classes observed at a pixel, T is the total number of time steps, and K is the total number of habitat classes. Higher PCI values indicate pixels that both change frequently and span multiple habitat states over time.

Seagrass structural dynamics

Temporal trends in benthic habitat composition were assessed using linear regression. Annual mapped area (km²) was regressed against year (2016–2025) separately for bare substrate, sparse and dense macroalgae, and sparse and dense seagrass. Regression slopes represented the annual rate of change in habitat area (km² year^{-1}), and statistical significance was evaluated at $\alpha = 0.05$. The proportion of deviance explained was used to assess model fit.

To quantify seagrass structural patterns and dynamics at the local scale, spatial pattern metrics (SPMs) were calculated across a regular sampling grid. We generated a 500 × 500 m fishnet grid from the raster extent, which served as a consistent spatial framework for extracting landscape metrics across the entire benthic habitat map time series. While this approach enabled standardized spatial and temporal comparisons, we recognize that SPMs are inherently sensitive to the size of analytical units (scale effect) and the positioning of their boundaries (zoning effect), as described by the modifiable areal unit problem (MAUP; Wong (2004)). SPMs were computed in R using the landscapemetrics package (Hesselbarth et al., 2019) for all habitat classes, but subsequent analyses focused on the dense seagrass class only, which significantly contributes to habitat structure and is most relevant to ecosystem functions and services (Callahan et al., 2026; Santos et al., 2016). To independently quantify changes in dense seagrass cover and fragmentation, we extracted the percentage of the landscape (PLAND) as a measure of seascape composition and habitat amount, and computed a composite fragmentation index (FRAG) developed by Santos et al. (2016) that integrates complementary aspects of spatial configuration:

$$FRAG = \left(\frac{LD \times PD \times AWMPAR}{GYRATE_{MN}}\right)^{1/4} \qquad (5)$$

where LD is landscape division and represents the degree of subdivision of the focal habitat class, PD is its patch density, AWMPAR is the area-weighted mean perimeter-to-area ratio of its patches, and GYRATE_MN is their mean radius of gyration. Higher FRAG values represent greater fragmentation, characterized by greater subdivision and patch density, increased patch shape complexity, and reduced patch spatial extent. The fragmentation index FRAG provides a comprehensive measure of fragmentation that increases with increasing disaggregation and edge complexity and decreases with greater patch compactness.

Then, two complementary measures of temporal change were evaluated: net change and cumulative change. Net change represented the overall difference between the last and first years of the time series and was calculated as:

$$\Delta X_{\text{net}} = X_{2025} - X_{2016} \qquad (6)$$

where X represents either PLAND or FRAG. Positive values indicate an overall increase in dense seagrass cover (PLAND) or fragmentation (FRAG) between 2016 and 2025, whereas negative values indicate an overall decrease. Values approaching zero indicate little difference between the beginning and end of the study period.

To incorporate the full temporal trajectory rather than only the two endpoint years, cumulative change was calculated as the sum of the absolute differences between consecutive years across the time series:

$$\Delta X_{\text{cum}} = \sum_{t=2016}^{2025} \left|\Delta X_{t,t-1}\right| \qquad (7)$$

This measure integrates year-to-year variation across the entire 2016–2025 time series, allowing areas characterized by persistent directional change to be distinguished from those exhibiting greater structural variability. Finally, net and cumulative PLAND and FRAG values were independently standardized using Z-scores to facilitate comparison of their distributions.

Results

Biscayne Bay SAV map time series

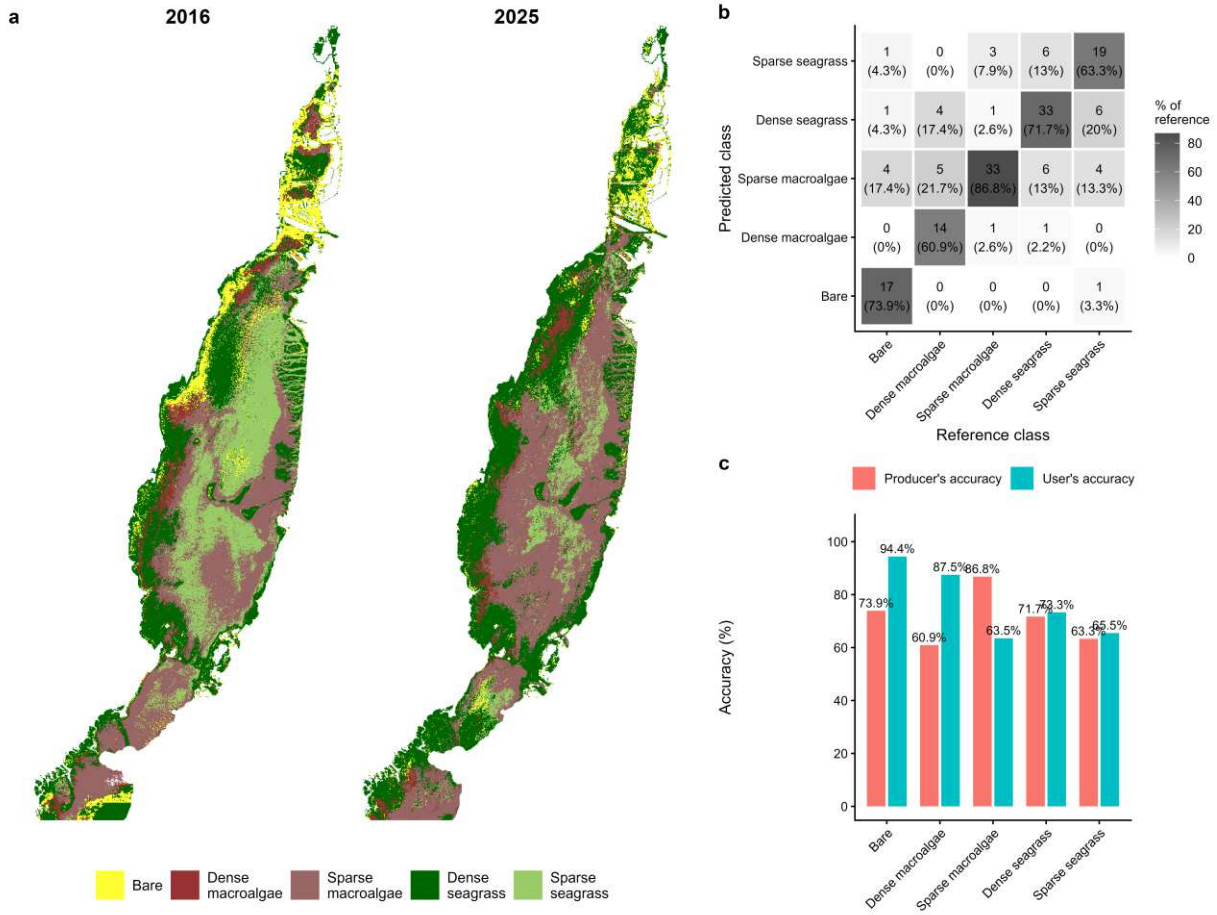


Figure 4: Benthic habitat mapping and classification performance in Biscayne Bay, Florida. (a) Benthic habitat maps for 2016 and 2025 showing five habitat classes based on SAV type and density. (b) Confusion matrix based on pooled independent validation observations. Cells show the number of observations and the percentage of each reference class assigned to each predicted class. (c) Class-specific producer's accuracy (PA) and user's accuracy (UA). Overall classification accuracy across pooled validation observations was 72.5%.

Our field-informed mapping approach successfully distinguished five benthic habitat classes across Biscayne Bay from 2016 to 2025 (Online Supplementary Material Fig. S1), achieving an overall classification accuracy of 72.5% based on pooled independent validation observations from 2023–2025 (Figure 4 b). Classification performance varied among habitat classes, with producer's accuracy highest for sparse macroalgae (86.8%), followed by bare substrate (73.9%), dense seagrass (71.7%), sparse seagrass (63.3%), and dense macroalgae (60.9%). User's accuracy was highest for bare substrate (94.4%) and dense macroalgae (87.5%), followed by dense seagrass (73.3%), sparse seagrass (65.5%), and sparse macroalgae (63.5%, Figure 4 c).

Benthic habitat distribution was spatially heterogeneous, with substantial differences between 2016 and 2025 (Figure 4 a). In 2016, sparse seagrass was broadly distributed throughout the central bay, whereas dense seagrass occurred primarily along the western and eastern margins and in portions of the northern and southern bay. By 2025, dense seagrass occupied a greater proportion of several areas previously characterized by sparse seagrass, particularly along the western margin and across portions of the southern bay. Macroalgal habitats remained extensive in the central bay, with sparse macroalgae occupying large areas and replacing the large extents of 2016 sparse seagrass by 2026. Dense macroalgae occurred in smaller, localized patches primarily in the western Bay nearby dense seagrass areas. Bare substrate was concentrated primarily in the northwestern bay and was less extensive elsewhere, decreasing between 2016 and 2026.

Pixel Change Index

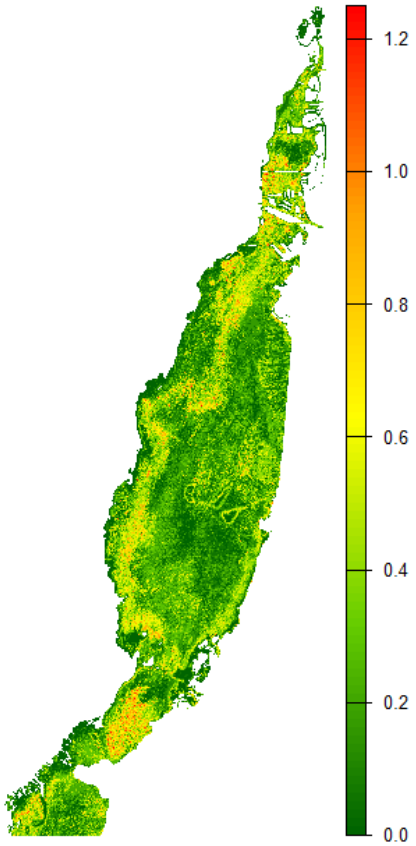


Figure 5: The Pixel Change Index (PCI) summarizes the frequency of habitat-class transitions across the 2016–2025 map series, with higher values indicating greater erratic pixel behavior in benthic habitat classification.

As expected, the Pixel Change Index (PCI) exhibited spatial heterogeneity in the frequency and diversity of benthic habitat transitions across Biscayne Bay (Figure 5). The central and eastern regions of the bay were characterized predominantly by low PCI values, generally ranging from approximately 0.1 to 0.3, indicating relatively few transitions among mapped habitat classes across the 2016–2025 time series. In contrast, moderate PCI values (approximately 0.4–0.6) were more prevalent along the western side of the bay, showing a prominent north-to-south swath of high habitat transitions nearshore. This swath showed the highest PCI values (>0.6) along with a hotspot in the southern bay. Within these areas, localized pixels reached values of approximately 0.8–1.0, with relatively few locations exceeding 1.0. Overall, the map was dominated by low to moderate PCI values, while areas of higher pixel variability concentrated in localized portions of the northern and southern bay, and along the western margin.

SAV compositional trajectory at the bay scale

Annual benthic habitat composition varied considerably across the study period, with the most pronounced fluctuations occurring in the relative extent of dense and sparse seagrass (Figure 6 a). Dense seagrass reached its maximum extent in 2018, followed by substantial interannual fluctuations, declining in 2024 before increasing again in 2025. Sparse seagrass exhibited broadly opposing fluctuations, reaching its greatest extent during 2023–2024 before declining sharply in 2025. Sparse macroalgae remained consistently abundant, whereas dense macroalgae represented a comparatively small proportion of the mapped area. Bare substrate declined until approximately 2020, followed by an increase in subsequent years. Despite substantial interannual fluctuations in habitat composition, the fitted linear models indicated no significant linear temporal trends across the study period (Figure 6 b, Table 1).

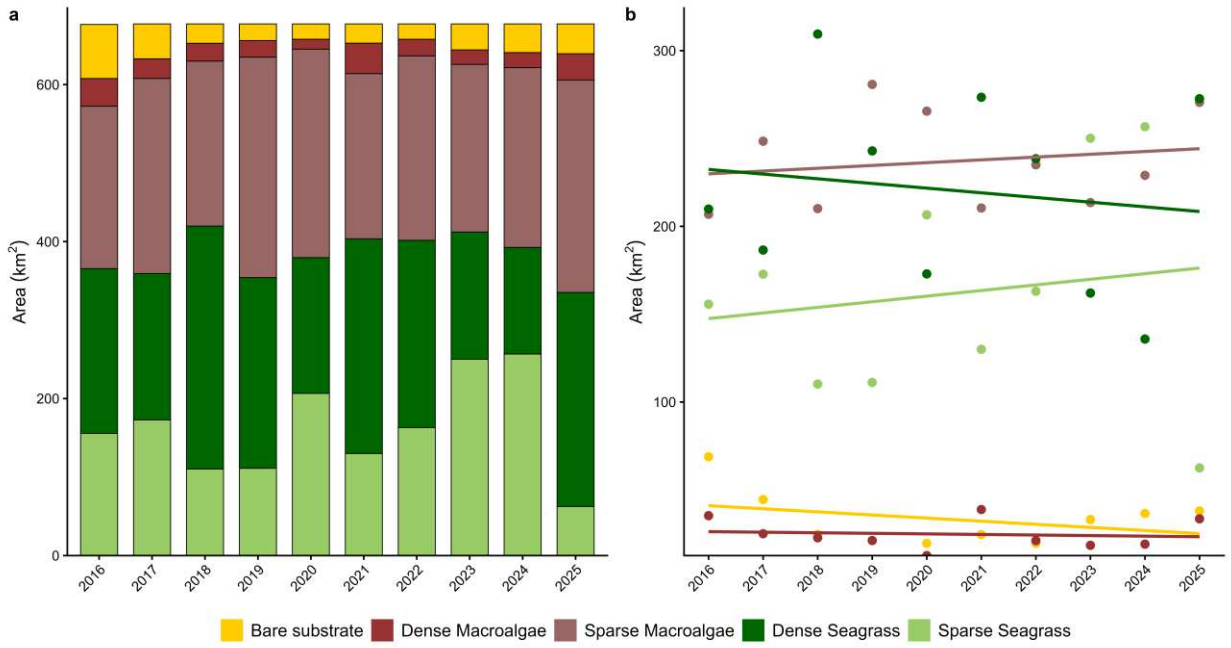


Figure 6: Temporal variation in benthic habitat composition across Biscayne Bay from 2016 to 2025. (a) Annual mapped area (km²) of the five benthic habitat classes shown as stacked bars. (b) Temporal trajectories in the area of each habitat class estimated using linear models (LM). Points represent the mapped area for each year, and lines represent the fitted temporal trends for each habitat class.

Table 1: Generalized additive model results for temporal variation in benthic habitat area from 2016 to 2025.

Habitat class	Estimate	T-value	p-value	Deviance explained (%)
Bare substrate	-1.76	-1.06	0.321	12.26
Dense Macroalgae	-0.32	-0.33	0.751	1.34
Sparse Macroalgae	1.59	0.50	0.632	3.00
Dense Seagrass	-2.66	-0.41	0.692	2.06
Sparse Seagrass	3.20	0.44	0.669	2.40

Spatial patterns of dense seagrass structural dynamics

Dense seagrass cover and fragmentation exhibited broadly inverse spatial patterns across Biscayne Bay in both 2016 and 2025, with areas of high PLAND generally characterized by lower FRAG (Figure 7 a,b,e,f). High dense

seagrass cover was consistently concentrated along the rim of the bay (particularly in the western rim), whereas lower PLAND characterized much of the deeper central interior. In contrast, elevated fragmentation was more spatially localized and occurred primarily in areas where dense seagrass cover was lower or less continuous, which included regions of the north central bay in 2016 and shifted to the south-central bay in 2025. This spatial correspondence was particularly apparent in the central and southern portions of the bay, where heterogeneous PLAND distributions coincided with higher FRAG values, while areas of extensive dense seagrass along the western margin and northern bay generally exhibited comparatively low fragmentation. Although the distribution of both metrics shifted regionally between 2016 and 2025, their broad inverse spatial relationship remained evident across the study period.

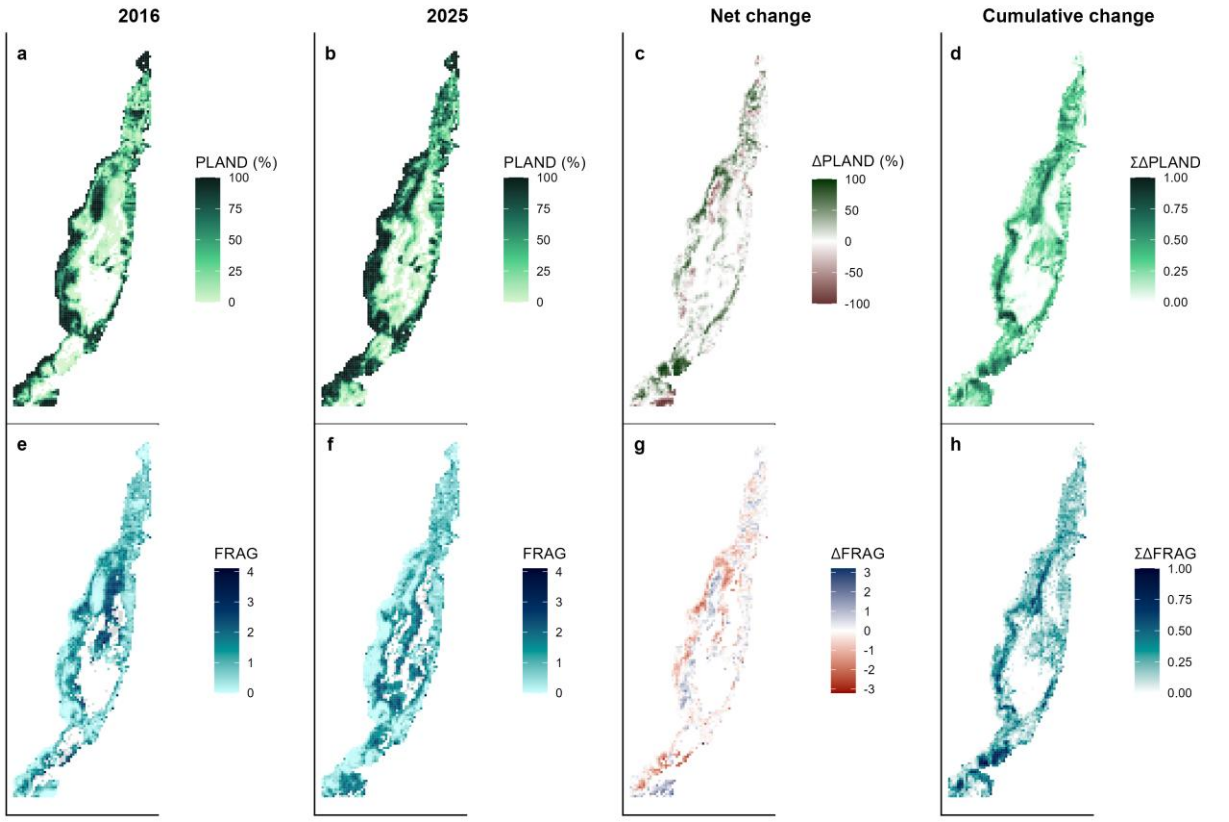


Figure 7: Spatial patterns and temporal changes in dense seagrass cover (PLAND) and fragmentation (FRAG) across Biscayne Bay (2016–2025). PLAND is shown for (a) 2016, (b) 2025, (c) net change, and (d) cumulative annual change. Corresponding FRAG metrics are shown in (e–h). Net change represents the difference between 2025 and 2016, whereas cumulative change represents the sum of consecutive annual differences. Positive values indicate increasing cover or fragmentation, respectively, and negative values indicate decreases. White cells indicate areas where dense seagrass was absent.

The inverse spatial relationship between dense seagrass cover and fragmentation was also evident in the net changes observed between 2016 and 2025, with increases in PLAND generally corresponding to decreases in FRAG and vice versa (Figure 7 c,g). This relationship was particularly pronounced along the western rim of the bay and southeastern areas, where localized losses in dense seagrass cover occurred alongside areas of substantial gain. Across the bay, mean net change was 8.79 for PLAND and −0.13 for FRAG. The standardized distributions further revealed differences in how net changes were distributed across the study system (Figure 8 a). PLAND exhibited a slightly negative median and a pronounced positive tail, indicating that most grid cells were concentrated near or below the mean net PLAND change, while a smaller subset experienced changes substantially above the mean. FRAG exhibited a slightly positive median and greater spread on both sides of the mean, with particularly long tails indicating that a small number of grid cells experienced changes substantially greater in magnitude than those observed across most of the bay. Together, our maps and standardized distributions show that changes in dense seagrass cover were generally accompanied by opposing changes in fragmentation, while the extended tails of both

distributions, particularly for FRAG, highlight localized areas where structural changes were substantially greater than across the broader seascape.

Cumulative changes in PLAND and FRAG revealed widespread temporal variability that was not fully captured by net differences between 2016 and 2025, particularly in seagrass spatial configuration (Figure 7 d,h). Cumulative changes in dense seagrass cover (PLAND) and fragmentation (FRAG) revealed widespread temporal variability that was not fully captured by net differences between 2016 and 2025, particularly in seagrass spatial configuration (Figure 7 d,h). Cumulative PLAND changes were elevated along a prominent north-to-south swath of the western bay, and in the smaller southern basins of the bay, indicating greater year-to-year fluctuations in dense seagrass cover throughout the study period (Figure 7 d). In contrast, cumulative FRAG changes were more broadly distributed across the bay (Figure 7 h). Mean cumulative change was 139.35 for PLAND and 2.91 for FRAG. The standardized distributions were positively skewed for both metrics, with medians slightly below zero and extended positive tails (Figure 8 b). Thus, most 500-m grid cells exhibited cumulative changes below their respective means, whereas a smaller proportion experienced substantially greater temporal variability. This pattern was particularly pronounced for FRAG, whose long positive tail indicates that cumulative changes in spatial configuration were concentrated in a relatively small subset of grid cells, with some areas experiencing substantially greater reorganization than most of the bay. Together, these spatial and distributional patterns indicate that seagrass cover and fragmentation underwent repeated changes throughout the study period, with certain areas experiencing disproportionately large intermediate fluctuations despite relatively small differences between their initial and final conditions

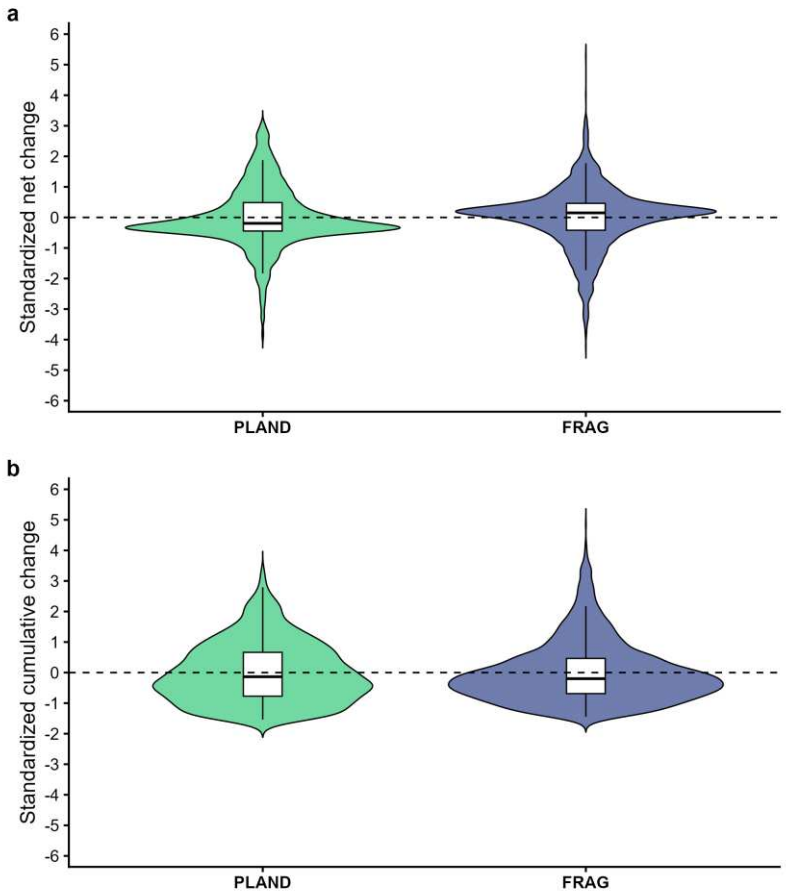


Figure 8: Distribution of standardized changes in dense seagrass cover and fragmentation across Biscayne Bay from 2016 to 2025. (a) Standardized net change in percentage of landscape occupied by dense seagrass (PLAND) and fragmentation (FRAG), calculated as the difference between 2025 and 2016. (b) Standardized cumulative change in PLAND and FRAG, calculated from the sum of absolute differences between consecutive annual observations. Distributions represent 500 randomly selected 500 × 500 m grid cells. Violin widths represent the density of observations, and inset boxplots show the median and interquartile range. Values were standardized separately within each metric;

therefore, zero represents the mean change for that metric, with positive and negative values representing changes above and below the respective mean.

Discussion

In this study, we developed an ecologically informed classification framework and applied it consistently across a Sentinel-2 archive to map continuous long-term seagrass dynamics in Biscayne Bay, Florida. Importantly, rather than reducing the system to a binary seagrass–non-seagrass representation, our model distinguished habitat classes according to vegetation cover and dominant SAV type. Binary classifications are effective for quantifying seagrass distribution and extent but can overlook the heterogeneity of SAV composition, where seagrasses occur across gradients of cover and alongside ecologically important macroalgal communities (Knudby & Nordlund, 2011; Lirman et al., 2014). Finer thematic resolution can therefore provide additional information on variation in seagrass density and composition that is not retained when SAV is represented as a single habitat class. Maintaining these distinctions was particularly relevant in our study site because a binary classification would have combined sparse and dense seagrass and macroalgal habitats, preventing us from consistently isolating dense seagrass through time. Our 5-class thematic resolution was supported by spectral clustering, which identified ecologically meaningful differences in SAV structure while remaining compatible with the spectral information available from Sentinel-2. Applying this framework across the ten-year Sentinel-2 archive revealed spatially heterogeneous SAV dynamics, with pronounced local changes in seagrass structure despite the absence of significant bay-wide temporal trends in SAV composition. At the bay scale, bare substrate exhibited a distinct temporal pattern, declining between 2016 and 2020 before gradually increasing through 2025. Together, these findings suggest considerable interannual variability in benthic habitat composition despite the absence of consistent directional trends among SAV classes. Such variability may reflect spatially heterogeneous changes, whereby increases in habitat extent in some areas offset declines elsewhere. At a finer spatial scale, areas experiencing increases in seagrass cover generally exhibited reduced fragmentation, suggesting the expansion and coalescence of existing patches, whereas declines in cover were frequently accompanied by greater fragmentation, consistent with the subdivision and isolation of remaining habitat. The cumulative analyses of dense seagrass cover and fragmentation revealed that habitat configuration does not always follow directional trajectories between end points, with some areas undergoing substantial year-to-year reorganization despite relatively small net changes over the study period. These findings highlight how seagrass structural dynamics can be overlooked when comparing only the beginning and end of a monitoring period, emphasizing the value of annual mapping for characterizing seascape dynamics. The occurrence of these changes in historically disturbed areas further highlighted the ecological relevance of the patterns detected. Together, our results show the value of systematically processing satellite imagery archives to produce consistent multi-class habitat maps, revealing temporal trajectories and spatial reorganization that may go undetected when analyses are limited to isolated observations or endpoint comparisons.

Temporal variability in SAV composition and habitat transitions

The Pixel Change Index (PCI) revealed spatially heterogeneous patterns of benthic habitat transitions across Biscayne Bay, with elevated values concentrated in a north–south swath along the western rim. These areas overlap with locations affected by documented environmental disturbances, including seagrass die-offs, macroalgal blooms, and changes in freshwater delivery associated with hydrological alterations (Carbonell et al., 2021; Collado-Vides et al., 2013; Lirman et al., 2014). The spatial correspondence between elevated PCI values and historically disturbed areas suggests that repeated transitions among benthic habitat classes may reflect ecologically meaningful variability in SAV communities. Thus, the PCI provides a spatially explicit characterization of areas experiencing recurrent habitat transitions, offering a basis for interpreting temporal SAV patterns in the context of Biscayne Bay's disturbance history. However, not all pixel-level transitions can necessarily be attributed to ecological processes, as PCI also incorporates uncertainty inherent in satellite-based benthic habitat classification. Complex water-column optical properties, depth, atmospheric and surface conditions, and spectral overlap among benthic classes can introduce variability in mapped class assignments (Dekker et al., 2005; Rowan & Kalacska, 2020; Veettil et al., 2020). This limitation is particularly relevant to transitions between sparse and dense seagrass, which represent differences along a continuum of vegetation cover rather than distinctly separated habitat types. Consequently, relatively small variations in vegetation density or spectral conditions may result in changes in categorical assignments, making it difficult to distinguish genuine ecological transitions from classification variability at the pixel level. Nevertheless, the correspondence between elevated PCI values and historically disturbed areas supports

the ecological relevance of the broader spatial patterns, while recognizing that individual transitions may reflect classification uncertainty.

Our ten-year compositional analysis provides a broader context for the localized habitat transitions captured by the PCI by evaluating SAV extent across the entire bay. Dense and sparse seagrass exhibited pronounced and often opposing fluctuations in mapped extent, suggesting potential interannual redistribution between these two classes. Although some of this variability may arise from classification uncertainty, transitions between density classes are also consistent with ecological processes affecting vegetation cover, including meadow thinning and increasing vegetation density, rather than complete habitat loss or recolonization. Studies across different coastal systems have demonstrated that seagrass cover and density vary substantially in response to environmental conditions across multiple spatiotemporal scales. In Moreton Bay, Australia, Roelfsema et al. (2014) examined changes in seagrass percentage cover over nine years (2004–2013), documenting an apparent increase in high-density seagrass (70–100% cover) and differences in temporal variability among individual banks. In Zanzibar, Tanzania, Alonso Aller et al. (2019) documented substantial declines followed by recovery in seagrass cover, with contrasting trajectories among closely spaced monitoring locations. Together, these findings provide ecological context for the opposing fluctuations in dense and sparse seagrass observed in this study, suggesting that changes in mapped extent of dense and sparse seagrass may reflect variations in vegetation abundance and meadow condition.

In Biscayne Bay, vegetation abundance and composition respond to spatial and temporal variation in environmental conditions, including freshwater delivery, salinity, nutrient availability, and disturbance occurring across multiple scales (Lirman et al., 2014; Santos et al., 2016; Santos et al., 2020). Importantly, environmental influences are spatially heterogeneous across Biscayne Bay and can produce substantial local changes in SAV without generating equivalent trends at broader spatial scales. Therefore, the absence of significant bay-wide trends in dense and sparse seagrass extent should not be interpreted as an absence of ecological change, but rather considered in relation to the spatial scale of analysis. Our results highlight this scale dependence, as local habitat transitions and interannual fluctuations can occur without producing persistent trends at the bay-wide level. Bare substrate exhibited a different temporal pattern, with an initial decline in mapped extent between 2016 and approximately 2020, followed by an increase toward the end of the study period. Although this pattern was evident in the annual habitat maps, the linear regression characterized only the overall tendency. However, the expansion of bare substrate is ecologically relevant because transitions from vegetated to unvegetated states can accompany disturbance-driven seagrass loss and may alter the continuity and spatial structure of SAV seascapes (Santos et al., 2016; Santos et al., 2020). In Biscayne Bay, previous disturbances have produced substantial reductions in seagrass cover and increased fragmentation, demonstrating that changes in vegetation extent can reorganize benthic habitat over relatively short periods (Santos et al., 2020). The increase in bare substrate during the latter portion of our time series may therefore indicate losses of vegetated habitat in certain areas of the bay; however, the absence of a significant trend within any single SAV class suggests that this system-wide trajectory was not attributable to sustained losses of one vegetation type alone.

Overall, interannual fluctuations among SAV classes and the spatial heterogeneity revealed by the PCI emphasize the importance of considering spatial scale when interpreting temporal changes in benthic habitat composition. Bay-wide analyses summarize the net extent of each habitat class, potentially masking local trajectories occuring across different portions of the study system.

Spatial patterns of dense seagrass cover and fragmentation

In contrast with the results of our bay-wide analysis, the 500-m grid revealed finer-scale spatial and temporal variation in seagrass structure, with distinct patterns in habitat composition and configuration. These dimensions were quantified independently because changes in habitat amount do not necessarily correspond to changes in its spatial arrangement, and seascapes with similar amounts of seagrass can exhibit substantially different configurations (Frazier & Kedron, 2017; Kupfer, 2012). In Biscayne Bay, however, PLAND and FRAG exhibited a pronounced inverse spatial relationship: areas with greater dense seagrass cover were generally less fragmented, whereas areas with lower cover exhibited greater fragmentation. This relationship was also apparent through time, as increases in dense seagrass cover frequently coincided with decreasing fragmentation, and vice versa. These patterns are consistent with the expansion and coalescence of dense seagrass patches where cover increased and greater subdivision of habitat where cover declined (Bell, 1999). Similar associations between seagrass loss and changes in spatial configuration have been documented in Biscayne Bay, where macroalgal blooms have contributed to reductions in seagrass cover and increased fragmentation (Santos et al., 2020), and altered freshwater delivery has influenced seagrass patch structure (Stipek et al., 2020) . Evidence from other seagrass ecosystems further illustrates

how changes in habitat extent can influence fragmentation. In southeastern Australia, Swadling et al. (2023) demonstrated that fragmentation of *Posidonia australis* meadows was associated with anthropogenic disturbances, particularly coastal urbanization and marine infrastructure, with boat mooring density emerging as an important predictor of habitat fragmentation. Similarly, Montefalcone et al. (2010) documented greater fragmentation of *Posidonia oceanica* meadows in human-impacted areas of the Mediterranean compared with relatively undisturbed sites, highlighting the influence of anthropogenic pressures on seagrass meadow configuration. These findings suggest that although habitat loss is often accompanied by spatial reorganization, the resulting fragmentation patterns depend on how habitat is distributed and subsequently lost. Indeed, Santos et al. (2016) demonstrated that seagrass habitat loss and fragmentation can follow independent trajectories, with some areas experiencing increased fragmentation despite relatively stable habitat cover. Therefore, although our results revealed a broadly inverse relationship between dense seagrass cover and fragmentation at the 500 × 500 m grid-cell scale, this association may differ at other spatial scales, where localized changes in habitat amount and configuration may be decoupled. This reinforces the importance of considering both dimensions of seagrass structure, as changes in habitat cover alone may not fully capture spatial reorganization within the seascape.

Net and cumulative changes in seagrass structure

Our annual mapping approach allowed seagrass dynamics to be examined at different temporal resolutions by contrasting net change over the ten-year study period with the cumulative magnitude of year-to-year changes occurring within that period. This distinction was particularly pronounced for FRAG, where substantial cumulative change occurred even in locations with relatively small net change, indicating repeated spatial reorganization that was not apparent from endpoint comparisons. In contrast, PLAND exhibited greater correspondence between net and cumulative patterns, suggesting comparatively more directional changes in dense seagrass cover. These findings reinforce the importance of temporal resolution in characterizing seagrass change, as time-series studies have shown that relatively similar conditions between endpoints can encompass substantial intermediate variability and nonlinear trajectories of decline, persistence, and recovery (Davies et al., 2024; Dunic, 2023). For instance, Lyons et al. (2013) analyzed 23 years of annual seagrass maps alongside a higher-frequency monthly time series in Moreton Bay, Australia, revealing that total seagrass area remained relatively stable despite significant declines in vegetation cover condition. Their findings reinforce how assessments based on changes in habitat extent alone can overlook important changes in seagrass condition and temporal dynamics. In our study, this was particularly evident for habitat configuration, where relatively limited net change sometimes concealed substantial cumulative variability over the study perios. Thus, similar habitat configurations at two points in time do not necessarily indicate structural stability throughout the intervening period. Consequently, evaluating cumulative changes alongside net changes highlights the value of continuous, long-term remote sensing monitoring, as repeated observations are essential for capturing seagrass dynamics and spatial reorganization that may remain undetected when relying solely on comparisons between individual time points.

Importantly, these temporal dynamics were not distributed uniformly across Biscayne Bay. Areas exhibiting pronounced changes in dense seagrass structure frequently overlapped with locations characterized by elevated PCI and a history of ecological disturbance, suggesting that the observed structural changes may reflect localized processes of habitat loss and subsequent recovery. Some of the strongest increases in dense seagrass cover and corresponding reductions in fragmentation occurred in northern and northwestern-central portions of the bay, where elevated PCI values coincided with areas previously affected by substantial ecological disturbances. Specifically, northern Biscayne Bay experienced a severe seagrass die-off that began in 2011 and intensified over subsequent years, peaking in 2017 when much of the seagrass habitat in the affected area had been lost (Alexandre et al., 2021; Carbonell et al., 2021). In the central-northwestern bay, persistent blooms of the macroalga *Anadyomene* spp. have contributed to seagrass decline by forming extensive algal cover over seagrass meadows, reducing meadow extent and limiting seagrass growth (Collado-Vides et al., 2013). Along the western shoreline, seagrass communities have been exposed to decades of hydrological alteration associated with the extensive canal and water-management network. These modifications replaced historically diffuse freshwater inputs with concentrated and often pulsed canal discharges, altering the quantity, timing, and distribution of freshwater entering the bay, causing strong fluctuations in salinity near canal mouths. These modified freshwater and salinity regimes have, in turn, influenced the abundance, composition, and spatial distribution of SAV along the western shoreline. Such disturbances can reduce vegetation cover, disrupt meadow continuity, and increase habitat fragmentation, leaving a spatially heterogeneous mosaic of remnant seagrass patches and unvegetated or sparsely vegetated areas (Lirman et al., 2014; Lirman & Cropper, 2003; Santos et al., 2016). Subsequent recolonization, vegetative expansion, or increases in shoot density may progressively reconnect these patches, increasing the proportion of dense seagrass habitat while

reducing fragmentation. Accordingly, the increasing PLAND and declining FRAG observed in portions of these historically disturbed areas are consistent with meadow expansion and coalescence following earlier habitat losses. The elevated PCI values further suggest that these areas experienced repeated changes in benthic habitat composition during the study period, potentially reflecting transitions between degraded and recovering vegetation states. Together, these findings suggest that the structural dynamics detected by our multitemporal mapping approach capture spatially heterogeneous trajectories of seagrass reorganization and possible recovery within historically disturbed portions of Biscayne Bay.

Implications for long-term SAV monitoring and management

The growing availability of long-term satellite archives provides an important opportunity to shift seagrass monitoring from individual mapping efforts toward automated and repeatable assessments of habitat dynamics. Recent studies have demonstrated the potential of developing classification models that can be systematically applied across satellite archives to reconstruct seagrass dynamics through time. For example, Davies et al. (2024) applied a neural network model to 471 Sentinel-2 images to characterize intertidal seagrass trajectories across six sites in Western Europe, while Callahan et al. (2026) trained a Random Forest model and back-cast it across a Sentinel-2 archive to characterize seasonal and interannual seagrass dynamics in Western Port, Australia. Building on this emerging framework, we applied a consistent Random Forest classification model across a ten-year Sentinel-2 data time series of Biscayne Bay while refining the thematic resolution of the resulting maps into five classes representing bare substrate and differences in SAV type and cover. This approach allowed the satellite archive to be systematically converted into a consistent time series of benthic habitat maps from which changes in habitat composition, configuration, and temporal dynamics could be quantified.

Developing scalable methods for systematically processing and classifying satellite imagery has direct relevance for coastal management, as standardized remote sensing workflows can support consistent, repeatable assessments of seagrass distribution and change across large spatial extents (Coffer et al., 2023; Traganos et al., 2018). Rather than relying exclusively on individual habitat maps or discrete mapping campaigns, these approaches can leverage existing and continuously growing Earth-observation archives to reconstruct past habitat trajectories and incorporate new observations as imagery becomes available. Such time series can help distinguish persistent habitat loss from short-term variability, identify areas undergoing recurrent structural reorganization, and detect potential recovery following disturbance. Retaining distinctions among SAV types and cover states further provides information on changes in habitat condition that may be obscured by binary seagrass–non-seagrass classifications. The continued development of automated and transferable classification workflows therefore provides a pathway for transforming satellite data into operational monitoring tools that can support the prioritization of habitat conservation, restoration, and other management actions.

Conclusions

In conclusion, seagrass dynamics in Biscayne Bay were characterized not simply by gains and losses in habitat extent, but by spatially heterogeneous trajectories involving changes in benthic composition, habitat amount, and spatial configuration through time. Applying a consistent multiclass classification framework across a ten-year Sentinel-2 archive allowed us to retain ecologically relevant differences in SAV type and cover while isolating stable seagrass habitat and examining change from complementary spatial and temporal perspectives. Although interannual and localized variability across the bay, these dynamics did not necessarily translate into directional system-wide trends, demonstrating that relatively stable habitats at broad scales can coexist with considerable local reorganization. Similarly, cumulative analyses revealed repeated changes in dense seagrass structure that were obscured by endpoint comparisons, particularly for fragmentation, where relatively small net differences obscured intermediate variability. The spatial correspondence of these patterns with the documented disturbance history of Biscayne Bay further provides ecological context for the dynamics detected from our benthic maps and identifies areas of potential habitat recovery and structural reorganization. Together, integrating pixel-level transitions with compositional and configurational metrics demonstrates the value of moving beyond individual habitat maps toward scalable approaches that systematically extract ecological information from satellite archives. Such frameworks can transform increasingly extensive Earth-observation records into temporally explicit assessments of habitat trajectories, providing a stronger basis for identifying persistent decline, recurrent change, and potential recovery by supporting long-term monitoring and management of dynamic seagrass seascapes.

Supplementary Information

The online version of this article contains supplementary material. A DOI link to the supplementary information will be provided upon publication.

Acknowledgments

We thank the members of the Santos Seascape Ecology Lab for their support and contributions to this research. We are particularly grateful to Carlos Pulido, Jessika Reyes, Christine Nation, and the Florida Fish and Wildlife Conservation Commission (FWC) Seagrass Integrated Mapping and Monitoring (SIMM) program team for their valuable assistance during fieldwork.

Author contributions

CRediT Taxonomy for Authorship Contributions: MC, JRR, WRJ, GAB, SMG, DG, JSR, ROS. All listed authors have agreed to be included and have approved the submitted version of this manuscript. MC led writing of the original draft and contributed to conceptualization, data curation, formal analysis, funding acquisition, project administration, and software; JRR, WRJ, and ROS contributed to conceptualization, data curation, formal analysis, funding acquisition, project administration, resources, software, and supervision; DG contributed to conceptualization, formal analysis, resources, software, and supervision; JSR contributed to conceptualization, funding acquisition, project administration, and supervision; GAB contributed to data curation and project administration; SMG contributed to data curation; and MC, JRR, WRJ, GAB, DG, JSR, and ROS contributed to investigation, methodology, validation, visualization, and review and editing of the manuscript.

Funding

This manuscript is the result of research funded by the United States Environmental Protection Agency (USEPA GRANT ID: SF-02D21022-0) and conducted in collaboration with projects supported by NSF (DEB-1832229, HRD-1547798, HRD-2111661), and FIU's Institute of Environment under award NA21NOS4780150 through the South Florida–Caribbean Cooperative Ecosystems Studies Unit. NSF Grants HRD-1547798 and HRD-2111661 were awarded to Florida International University as part of the Centers of Research Excellence in Science and Technology (CREST) Program. This is contribution #XXX in the Institute of Environment at Florida International University.

Data availability

Once accepted for publication, all data and code will be publicly available on GitHUB and archived on Zenodo.

Declarations

Ethical approval

No animal testing was performed during this study.

Conflict of Interest

The authors declare that they have no conflict of interest.

Competing interests

The authors declare no competing interests.

Sampling and field studies

Field sampling was conducted under Florida Fish and Wildlife Conservation Commission permit SAL-24-2510-SR and Biscayne National Park permit BISC-2025-SCI-0012.

References

Alexandre, A., Collado-Vides, L., & Santos, R. (2021). The takeover of *Thalassia testudinum* by *anadyomene* sp. At Biscayne Bay, USA, cannot be simply explained by competition for nitrogen and phosphorous. *Marine Pollution Bulletin*, *167*, 112326. https://doi.org/10.1016/j.marpolbul.2021.112326

Alonso Aller, E., Eklöf, J. S., Gullström, M., Kloiber, U., Linderholm, H. W., & Nordlund, L. M. (2019). Temporal variability of a protected multispecific tropical seagrass meadow in response to environmental change. *Environmental Monitoring and Assessment*, *191*(12), 774. https://doi.org/10.1007/s10661-019-7977-z

Aybar, C., & Stigler, M. (2021). *Rgee: R Bindings for Calling the 'Earth Engine' API*. https://doi.org/10.32614/CRAN.package.rgee

Bell, S. S. (1999). Gap Dynamics in a Seagrass Landscape. *Ecosystems*, *2*(6), 493–504. https://doi.org/10.1007/s100219900097

Bischl, B., Lang, M., Kotthoff, L., Schiffner, J., Richter, J., Studerus, E., Casalicchio, G., & Jones, Z. M. (2016). Mlr: Machine Learning in R. *Journal of Machine Learning Research*, *17*(170), 1–5. http://jmlr.org/papers/v17/15-066.html

Boström, C., Pittman, S., Simenstad, C., & Kneib, R. (2011). Seascape ecology of coastal biogenic habitats: Advances, gaps, and challenges. *Marine Ecology Progress Series*, *427*, 191–217. https://doi.org/10.3354/meps09051

Breiman, L., Cutler, A., Liaw, A., & Wiener, M. (2002). *randomForest: Breiman and Cutlers Random Forests for Classification and Regression*. https://doi.org/10.32614/CRAN.package.randomForest

Browder, J. A., & Ogden, J. C. (1999). The natural South Florida system II: Predrainage ecology. *Urban Ecosystems*, *3*(3), 245–277. https://doi.org/10.1023/A:1009504601357

Caccia, V., Janz, E. M., Estevanez, M., & Olascoaga, M. J. (2026). Climate change influence on salinity, temperature, dissolved oxygen and pH in Biscayne Bay (Florida): Two decades of observations (2001–2021). *Estuarine, Coastal and Shelf Science*, *336*, 109861. https://doi.org/10.1016/j.ecss.2026.109861

Callahan, L., Dalby, O., Coleman, R. A., Young, M. A., Ierodiaconou, D., & Sherman, C. D. (2026). Temporal seagrass mapping using machine learning and field-validated satellite imagery to inform restoration and management. *Environmental Advances*, *23*, 100686. https://doi.org/10.1016/j.envadv.2026.100686

Carbonell, A., Joykutty, L., & Velde, B. (2021). Seagrass fatalities in North Biscayne Bay, South Florida due to increases in nutrients and macroalgae in its environment. *Journal of Student Research*, *10*(3). https://doi.org/10.47611/jsrhs.v10i3.1599

Coffer, M. M., Graybill, D. D., Whitman, P. J., Schaeffer, B. A., Salls, W. B., Zimmerman, R. C., Hill, V., Lebrasse, M. C., Li, J., Keith, D. J., Kaldy, J., Colarusso, P., Raulerson, G., Ward, D., & Kenworthy, W. J. (2023). Providing a framework for seagrass mapping in United States coastal ecosystems using high spatial resolution satellite imagery. *Journal of Environmental Management*, *337*, 117669. https://doi.org/10.1016/j.jenvman.2023.117669

Collado-Vides, L., Avila, C., Blair, S., Leliaert, F., Rodriguez, D., Thyberg, T., Schneider, S., Rojas, J., Sweeney, P., Drury, C., & Lirman, D. (2013). A persistent bloom of Anadyomene J.V. Lamouroux (Anadyomenaceae, Chlorophyta) in Biscayne Bay, Florida. *Aquatic Botany*, *111*, 95–103. https://doi.org/10.1016/j.aquabot.2013.06.010

Cunha, A. H., & Santos, R. P. (2009). The use of fractal geometry to determine the impact of inlet migration on the dynamics of a seagrass landscape. *Estuarine, Coastal and Shelf Science*, *84*(4), 584–590. https://doi.org/10.1016/j.ecss.2009.07.030

Davies, B. F. R., Oiry, S., Rosa, P., Zoffoli, M. L., Sousa, A. I., Thomas, O. R., Smale, D. A., Austen, M. C., Biermann, L., Attrill, M. J., Roman, A., Navarro, G., Barillé, A.-L., Harin, N., Clewley, D., Martinez-Vicente, V., Gernez, P., & Barillé, L. (2024). Intertidal seagrass extent from Sentinel-2 time-series show distinct trajectories in Western Europe. *Remote Sensing of Environment*, *312*, 114340. https://doi.org/10.1016/j.rse.2024.114340

Dekker, A. G., Brando, V. E., & Anstee, J. M. (2005). Retrospective seagrass change detection in a shallow coastal tidal Australian lake. *Remote Sensing of Environment*, *97*(4), 415–433. https://doi.org/10.1016/j.rse.2005.02.017

Dunic, J. (2023). *Understanding the effect of multiple stressors using seagrass as a model system*. https://summit.sfu.ca/item/36203

Fahrig, L., Baudry, J., Brotons, L., Burel, F. G., Crist, T. O., Fuller, R. J., Sirami, C., Siriwardena, G. M., & Martin, J.-L. (2011). Functional landscape heterogeneity and animal biodiversity in agricultural landscapes. *Ecology Letters*, *14*(2), 101–112. https://doi.org/10.1111/j.1461-0248.2010.01559.x

Fernandes, M. B., Hennessy, A., Law, W. B., Daly, R., Gaylard, S., Lewis, M., & Clarke, K. (2022). Landsat historical records reveal large-scale dynamics and enduring recovery of seagrasses in an impacted seascape. *Science of The Total Environment*, *813*, 152646. https://doi.org/10.1016/j.scitotenv.2021.152646

Floyd, M., East, H. K., & Suggitt, A. J. (2026). Evaluating methods for high-resolution, national-scale seagrass mapping in Google Earth Engine. *Remote Sensing in Ecology and Conservation*, *12*(2), 292–304. https://doi.org/10.1002/rse2.70039

Frazier, A. E., & Kedron, P. (2017). Landscape Metrics: Past Progress and Future Directions. *Current Landscape Ecology Reports*, *2*(3), 63–72. https://doi.org/10.1007/s40823-017-0026-0

Heide, T. van der, Bouma, T. J., Nes, E. H. van, Koppel, J. van de, Scheffer, M., Roelofs, J. G. M., Katwijk, M. M. van, & Smolders, A. J. P. (2010). Spatial self-organized patterning in seagrasses along a depth gradient of an intertidal ecosystem. *Ecology*, *91*(2), 362–369. https://doi.org/10.1890/08-1567.1

Herrera-Silveira, J. A., Palafox-Juárez, E. B., Mendoza-Martínez, J. E., Montero Muñoz, J. L., & Teutli Hernandez, C. (2024). Landscape configuration in seagrass meadows and its influence on carbon stock on reef lagoon systems. *Frontiers in Marine Science*, *11*. https://doi.org/10.3389/fmars.2024.1320194

Hesselbarth, M. H. K., Sciaini, M., With, K. A., Wiegand, K., & Nowosad, J. (2019). Landscapemetrics: An open-source R tool to calculate landscape metrics. *Ecography*, *42*(10), 1648–1657. https://doi.org/10.1111/ecog.04617

Hijmans, R. J. (2020). *Terra: Spatial Data Analysis*. https://doi.org/10.32614/CRAN.package.terra

Hossain, M. S., Bujang, J. S., Zakaria, M. H., & Hashim, M. (2015). The application of remote sensing to seagrass ecosystems: An overview and future research prospects. *International Journal of Remote Sensing*, *36*(1), 61–114. https://doi.org/10.1080/01431161.2014.990649

Jensen, S., & Bell, S. (2001). Seagrass growth and patch dynamics: Cross-scale morphological plasticity. *Plant Ecology*, *155*(2), 201–217. https://doi.org/10.1023/A:1013286731345

Kaufman, L., & Rousseeuw, P. J. (2009). *Finding Groups in Data: An Introduction to Cluster Analysis*. John Wiley & Sons.

Kennedy, R. E., Yang, Z., & Cohen, W. B. (2010). Detecting trends in forest disturbance and recovery using yearly Landsat time series: 1. LandTrendr — Temporal segmentation algorithms. *Remote Sensing of Environment*, *114*(12), 2897–2910. https://doi.org/10.1016/j.rse.2010.07.008

Knudby, A., & Nordlund, L. (2011). Remote sensing of seagrasses in a patchy multi-species environment. *International Journal of Remote Sensing*, *32*(8), 2227–2244. https://doi.org/10.1080/01431161003692057

Krause, J. R., Hinojosa-Corona, A., Gray, A. B., & Burke Watson, E. (2021). Emerging Sensor Platforms Allow for Seagrass Extent Mapping in a Turbid Estuary and from the Meadow to Ecosystem Scale. *Remote Sensing*, *13*(18), 3681. https://doi.org/10.3390/rs13183681

Kuhn, M. (2007). *Caret: Classification and Regression Training*. https://doi.org/10.32614/CRAN.package.caret

Kuhwald, K., Schneider von Deimling, J., Schubert, P., & Oppelt, N. (2022). How can Sentinel-2 contribute to seagrass mapping in shallow, turbid Baltic Sea waters? *Remote Sensing in Ecology and Conservation*, *8*(3), 328–346. https://doi.org/10.1002/rse2.246

Kupfer, J. A. (2012). Landscape ecology and biogeography: Rethinking landscape metrics in a post-FRAGSTATS landscape. *Progress in Physical Geography: Earth and Environment*, *36*(3), 400–420. https://doi.org/10.1177/0309133312439594

Lirman, D., & Cropper, W. P. (2003). The influence of salinity on seagrass growth, survivorship, and distribution within Biscayne Bay, Florida: Field, experimental, and modeling studies. *Estuaries*, *26*(1), 131–141. https://doi.org/10.1007/BF02691700

Lirman, D., Thyberg, T., Santos, R., Schopmeyer, S., Drury, C., Collado-Vides, L., Bellmund, S., & Serafy, J. (2014). SAV Communities of Western Biscayne Bay, Miami, Florida, USA: Human and Natural Drivers of Seagrass and Macroalgae Abundance and Distribution Along a Continuous Shoreline. *Estuaries and Coasts*, *37*(5), 1243–1255. https://doi.org/10.1007/s12237-014-9769-6

Lyons, M. B., Roelfsema, C. M., & Phinn, S. R. (2013). Towards understanding temporal and spatial dynamics of seagrass landscapes using time-series remote sensing. *Estuarine, Coastal and Shelf Science*, *120*, 42–53. https://doi.org/10.1016/j.ecss.2013.01.015

Lyzenga, D. R., Malinas, N. P., & Tanis, F. J. (2006). Multispectral bathymetry using a simple physically based algorithm. *IEEE Transactions on Geoscience and Remote Sensing*, *44*(8), 2251–2259. https://doi.org/10.1109/TGRS.2006.872909

McGarigal, K. (1995a). *FRAGSTATS: Spatial Pattern Analysis Program for Quantifying Landscape Structure*. U.S. Department of Agriculture, Forest Service, Pacific Northwest Research Station.

McGarigal, K. (1995b). *FRAGSTATS: Spatial Pattern Analysis Program for Quantifying Landscape Structure*. U.S. Department of Agriculture, Forest Service, Pacific Northwest Research Station.

Montefalcone, M., Parravicini, V., Vacchi, M., Albertelli, G., Ferrari, M., Morri, C., & Bianchi, C. N. (2010). Human influence on seagrass habitat fragmentation in NW Mediterranean Sea. *Estuarine, Coastal and Shelf Science*, *86*(2), 292–298. https://doi.org/10.1016/j.ecss.2009.11.018

O'Brien, K. R., Waycott, M., Maxwell, P., Kendrick, G. A., Udy, J. W., Ferguson, A. J. P., Kilminster, K., Scanes, P., McKenzie, L. J., McMahon, K., Adams, M. P., Samper-Villarreal, J., Collier, C., Lyons, M., Mumby, P. J., Radke, L., Christianen, M. J. A., & Dennison, W. C. (2018). Seagrass ecosystem trajectory depends on the relative timescales of resistance, recovery and disturbance. *Marine Pollution Bulletin*, *134*, 166–176. https://doi.org/10.1016/j.marpolbul.2017.09.006

Pebesma, E. (2018). Simple features for r: Standardized support for spatial vector data. *The R Journal*. https://digitalcommons.unl.edu/r-journal/626

Pittman, S. J. (2017). *Seascape Ecology*. John Wiley & Sons.

Pu, R., Bell, S., Levy, K. H., & Meyer, C. (2010). Mapping detailed seagrass habitats using satellite imagery. *2010 IEEE International Geoscience and Remote Sensing Symposium*, 1–4. https://doi.org/10.1109/IGARSS.2010.5651884

Roca, G., Alcoverro, T., Krause-Jensen, D., Balsby, T. J. S., Van Katwijk, M. M., Marbà, N., Santos, R., Arthur, R., Mascaró, O., Fernández-Torquemada, Y., Pérez, M., Duarte, C. M., & Romero, J. (2016). Response of seagrass indicators to shifts in environmental stressors: A global review and management synthesis. *Ecological Indicators*, *63*, 310–323. https://doi.org/10.1016/j.ecolind.2015.12.007

Rodemann, J. R., James, W. R., Rehage, J. S., Furman, B. T., Pittman, S. J., & Santos, R. O. (2025). Response of submerged aquatic vegetation seascapes to a large-scale seagrass die-off: A case study in Florida Bay. *Estuarine, Coastal and Shelf Science*, *318*, 109221. https://doi.org/10.1016/j.ecss.2025.109221

Rodemann, J. R., James, W. R., Santos, R. O., Furman, B. T., Fratto, Z. W., Bautista, V., Lara Hernandez, J., Viadero, N. M., Linenfelser, J. O., Lacy, L. A., Hall, M. O., Kelble, C. R., Kavanagh, C., & Rehage, J. S. (2021). Impact of Extreme Disturbances on Suspended Sediment in Western Florida Bay: Implications for Seagrass Resilience. *Frontiers in Marine Science*, *8*. https://doi.org/10.3389/fmars.2021.633240

Roelfsema, C. M., Lyons, M., Kovacs, E. M., Maxwell, P., Saunders, M. I., Samper-Villarreal, J., & Phinn, S. R. (2014). Multi-temporal mapping of seagrass cover, species and biomass: A semi-automated object based image analysis approach. *Remote Sensing of Environment*, *150*, 172–187. https://doi.org/10.1016/j.rse.2014.05.001

Rowan, G., & Kalacska, M. (2020). *Remote sensing of submerged aquatic vegetation: An introduction and best practices review* [Preprint]. Open Science Framework. https://doi.org/10.31219/osf.io/2gpxz

Santos, R. O., Lirman, D., & Pittman, S. J. (2016). Long-term spatial dynamics in vegetated seascapes: Fragmentation and habitat loss in a human-impacted subtropical lagoon. *Marine Ecology*, *37*(1), 200–214. https://doi.org/10.1111/maec.12259

Santos, R. O., Varona, G., Avila, C. L., Lirman, D., & Collado-Vides, L. (2020). Implications of macroalgae blooms to the spatial structure of seagrass seascapes: The case of the *anadyomene* spp. (Chlorophyta) bloom in Biscayne Bay, Florida. *Marine Pollution Bulletin*, *150*, 110742. https://doi.org/10.1016/j.marpolbul.2019.110742

Sleeman, J. C., Kendrick, G. A., Boggs, G. S., & Hegge, B. J. (2005). Measuring fragmentation of seagrass landscapes: Which indices are most appropriate for detecting change? *Marine and Freshwater Research*, *56*(6), 851–864. https://doi.org/10.1071/MF04300

Stipek, C., Santos, R., Babcock, E., & Lirman, D. (2020). Modelling the resilience of seagrass communities exposed to pulsed freshwater discharges: A seascape approach. *PLOS ONE*, *15*(2), e0229147. https://doi.org/10.1371/journal.pone.0229147

Swadling, D. S., West, G. J., Gibson, P. T., Laird, R. J., & Glasby, T. M. (2023). Don't go breaking apart: Anthropogenic disturbances predict meadow fragmentation of an endangered seagrass. *Aquatic Conservation: Marine and Freshwater Ecosystems*, *33*(1), 56–69. https://doi.org/10.1002/aqc.3905

Taylor, M. D., Strydom, S., Fraser, M. W., Sequeira, A. M. M., & Kendrick, G. A. (2026). Breaking down seagrass fragmentation in a marine heatwave impacted World Heritage Area. *Remote Sensing in Ecology and Conservation*, *12*(2), 183–198. https://doi.org/10.1002/rse2.70032

Traganos, D., Aggarwal, B., Poursanidis, D., Topouzelis, K., Chrysoulakis, N., & Reinartz, P. (2018). Towards Global-Scale Seagrass Mapping and Monitoring Using Sentinel-2 on Google Earth Engine: The Case Study of the Aegean and Ionian Seas. *Remote Sensing*, *10*(8), 1227. https://doi.org/10.3390/rs10081227

Traganos, D., Lee, C. B., Blume, A., Poursanidis, D., Čižmek, H., Deter, J., Mačić, V., Montefalcone, M., Pergent, G., Pergent-Martini, C., Ricart, A. M., & Reinartz, P. (2022). Spatially explicit seagrass extent mapping across the entire mediterranean. *Frontiers in Marine Science*, *9*. https://www.frontiersin.org/articles/10.3389/fmars.2022.871799

Uhrin, A. V., & Turner, M. G. (2018). Physical drivers of seagrass spatial configuration: The role of thresholds. *Landscape Ecology*, *33*(12), 2253–2272. https://doi.org/10.1007/s10980-018-0739-4

Vanhellemont, Q., & Ruddick, K. (2016). *ACOLITE FOR SENTINEL-2: AQUATIC APPLICATIONS OF MSI IMAGERY*.

Veettil, B. K., Ward, R. D., Lima, M. D. A. C., Stankovic, M., Hoai, P. N., & Quang, N. X. (2020). Opportunities for seagrass research derived from remote sensing: A review of current methods. *Ecological Indicators*, *117*, 106560. https://doi.org/10.1016/j.ecolind.2020.106560

Waycott, M., Duarte, C. M., Carruthers, T. J. B., Orth, R. J., Dennison, W. C., Olyarnik, S., Calladine, A., Fourqurean, J. W., Heck, K. L., Hughes, A. R., Kendrick, G. A., Kenworthy, W. J., Short, F. T., & Williams, S. L. (2009). Accelerating loss of seagrasses across the globe threatens coastal ecosystems. *Proceedings of the National*

827 *Academy of Sciences of the United States of America*, *106*(30), 12377–12381.
828 https://doi.org/10.1073/pnas.0905620106

829 Wedding, L., Lepczyk, C., Pittman, S., Friedlander, A., & Jorgensen, S. (2011). Quantifying seascape structure:
830 Extending terrestrial spatial pattern metrics to the marine realm. *Marine Ecology Progress Series*, *427*, 219–232.
831 https://doi.org/10.3354/meps09119

832 Wong, D. W. S. (2004). The Modifiable Areal Unit Problem (MAUP). In D. G. Janelle, B. Warf, & K. Hansen
833 (Eds.), *WorldMinds: Geographical Perspectives on 100 Problems: Commemorating the 100th Anniversary of the*
834 *Association of American Geographers 1904–2004* (pp. 571–575). Springer Netherlands.
835 https://doi.org/10.1007/978-1-4020-2352-1_93

836 Yarnall, A. H., Byers, J. E., Yeager, L. A., & Fodrie, F. J. (2022). Comparing edge and fragmentation effects within
837 seagrass communities: A meta-analysis. *Ecology*, *103*(3), e3603. https://doi.org/10.1002/ecy.3603

Supplementary Files

This is a list of supplementary files associated with this preprint. Click to download.

- CoppolaSupplementaryInformationLandscEcol.pdf